Numerical Heat Transfer, Part A: Applications: An International Journal of Computation and Methodology
Publication details, including instructions for authors and subscription information:
http://www.tandfonline.com/loi/unht20

PROPAGATION OF THERMAL WAVES IN A COMPOSITE MEDIUM WITH INTERFACE THERMAL BOUNDARY RESISTANCE

Whey-Bin Lor, Hsin-Sen Chu
Published online: 29 Oct 2010.

To cite this article: Whey-Bin Lor, Hsin-Sen Chu (1999) PROPAGATION OF THERMAL WAVES IN A COMPOSITE MEDIUM WITH INTERFACE THERMAL BOUNDARY RESISTANCE, Numerical Heat Transfer, Part A: Applications: An International Journal of Computation and Methodology, 36:7, 681-697, DOI: 10.1080/104077899274516

To link to this article: http://dx.doi.org/10.1080/104077899274516

Numerical Heat Transfer, Part A, 36:681–697, 1999

1040–7782/99 $12.00 + .00

PROPAGATION OF THERMAL WAVES IN A COMPOSITE MEDIUM WITH INTERFACE THERMAL BOUNDARY RESISTANCE

Whey-Bin Lor and Hsin-Sen Chu
Department of Mechanical Engineering, National Chiao Tung University, Hsinchu, Taiwan 300, Republic of China

This article numerically analyzes the hyperbolic heat conduction problem in a two-layer composite medium under an initial temperature pulse emanating from the exterior surface of one layer. Reflection and transmission occur when the initial pulse wave impacts the contact surface of the dissimilar material. An interfacial layer with low conductivity and narrow thickness exists at the interface, which is employed to model the thermal boundary resistance at the contact surface. Analysis results indicate that the interface resistance significantly influences the wave pattern and strength. The presentation of the wave nature in the interfacial layer deforms the initial wave feature and induces secondary wavelets behind the reflected and transmitted wave. In addition, the piecewise secondary wavelets become smooth when the interfacial width is very thin. Also examined herein is the effect of conductivity and thickness width of the interfacial layer coupled with variation of the two-layer properties ratio on the reflection-transmission-combination phenomena.

INTRODUCTION

Among the variety of devices making use of composite materials are thin-film superconductors, microelectronic layer packages, and fins. The devices have numerous applications. Classical diffusion theory (Fourier's law) has been extensively applied toward the heat transfer problem in a composite medium, with results indicating that the contact thermal resistance seriously affects the heat transfer mechanism [1, 2].

Fourier's law analysis suggests that an infinite speed of propagation of the thermal wave yields reliable results for most circumstances. However, recent investigations involving an extremely low temperature near absolute zero, extremely short transient duration, and extremely high rate change of temperature or heat flux have indicated that the heat propagation velocity under such circumstances becomes finite and dominant [3–6]. While considering the finite speed of wave propagation, Cattaneo [7] and Vernotte [8] independently suggested a modified heat flux model in the form of

$$\mathbf{q}(\mathbf{r}, t + \tau) = -k\nabla T(\mathbf{r}, t) \tag{1}$$

Received 29 October, 1998; accepted 16 July, 1999.

The authors would like to thank the National Science Council of Taiwan for financially supporting this research under Contract No. NSC 88-2218-E-009-003. Dr. J. P. Wu is also appreciated for his valuable discussions.

Address correspondence to Professor Hsin-Sen Chu, Department of Mechanical Engineering, National Chiao Tung University, 1001 Ta Hsueh Road, Hsinchu, Taiwan 300, R.O.C. E-mail: hschu@cc.nctu.edu.tw.

NOMENCLATURE

c	thermal wave speed	τ	relaxation time
C_p	specific heat capacity		
D_r	interfacial layer thickness	**Subscripts**	
e	thermal incident energy		
k	thermal conductivity	ave	average
q	heat flux	i	control volume index
$\mathbf{q}$	heat flux vector	$i \pm 1/2$	value at control volume faces
$\mathbf{r}$	position vector	j	layer index
t	time	max	maximum
T	temperature	r	interfacial layer
T_{ref}	reference temperature	1	layer 1
	$(= ec_1/\rho_1 C_{p_1}\alpha_1)$	2	layer 2
T_0	initial temperature		
W	characteristics variable	**Superscripts**	
α	thermal diffusivity		
δx	skin depth	iter	iteration
ε_{d}	nondimensional incident energy	$n, n+1$	time levels n and $n+1$
λ	eigenvalue	$[\,]^{-1}$	inverse matrix
ρ	density	*	dimensionless variable

where τ is relaxation time, k the thermal conductivity, $\mathbf{r}$ the position vector, and t the physical time. According to Eq. (1) the temperature gradient established at time t results in a heat flux vector at a later time $t + \tau$ due to an insufficient response time. Actually, the relaxation time τ is associated with the communication "time" between phonons (phonon-phonon collisions) deemed necessary for commencement of the heat flow and is a measure of thermal inertia of the medium. Based on the collision theory of molecules, τ is approximated to α/c^2 [9], where c represents the thermal wave velocity and α is the thermal diffusivity. Clearly, for $\tau = 0$, Eq. (1) reduces to the classical diffusion theory, leading to an infinite propagation velocity. Several investigators [9–12] have estimated the magnitude of τ for engineering materials. Recently, Mitra et al. [13] determined experimentally the τ value to be ~ 16 s for a biological material and directly validated the hyperbolic nature of heat conduction.

While emphasizing engineering applications of thermal wave theory, Özisik and Tzou [14] thoroughly reviewed thermal wave propagation, including the sharp wave-front and rate effects, thermal shock phenomenon, and thermal resonance phenomena. Various analytical methods have been proposed to elucidate the reflection, refraction, and transmission of thermal waves across a material interface. Frankel et al. [15] proposed a flux formulation to investigate thermal waves in a composite medium. Tzou [16] performed harmonic analysis to examine the reflection and refraction thermal wave patterns from a surface and an interface between dissimilar material. Previous investigations did not consider thermal boundary resistance at the interface. Bai and Lavine [17] treated boundary resistance as a jump boundary condition of a thin layer, indicating that it significantly affects the thermal wave solution. To our knowledge, the reflection/transmission of thermal waves in a composite medium while considering the thermal boundary

resistance at the interface of contact surfaces has not yet been investigated in detail.

To predict the boundary resistance, Streiffer et al. [18] indicated that a significant thermal barrier exists at the superconductor film-substrate interface. Marshall et al. [19] reported that a thermal barrier significantly restricts heat transfer from the film into the substrate. Das and Sadhal [20, 21] developed a model for two solids in contact with a finite thickness gap to evaluate the thermal constriction resistance. In this study, the interfacial layer model is employed to consider the thermal boundary resistance at the contact interface of two dissimilar materials. This model assumes an interfacial layer of variable thickness and conductivity in between the two different layers. The influence of interface resistance on the wave propagating in a composite medium under an initial pulsed temperature wave emanating from one layer is examined. The results demonstrate that the interface resistance heavily influences the reflected and transmitted wave patterns and related strengths.

PHYSICAL MODEL AND THEORETICAL ANALYSIS

Figure 1 depicts the composite medium, which consists of two different materials: layer 1 and layer 2. To predict the thermal boundary resistance, an interfacial layer of a variable thickness D_r with low conductivity k_r in between the two different layers is assumed. A pulsed incident energy e is exerted on the front surface of layer 1 and is absorbed within a skin depth of δx of layer 1. At time $= 0^+$ the thermal energy within δx is released and then emanates into the second layer.

By applying Taylor's series expansion to $\mathbf{q}$ in Eq. (1) with respect to τ, the linearized constitutive equation and energy conservation equations are written as

$$q(x, t) + \tau \frac{\partial q(x, t)}{\partial t} = -k \nabla T(x, t) \tag{2}$$

$$\rho C_p \frac{\partial T(x, t)}{\partial t} + \nabla q(x, t) = 0 \tag{3}$$

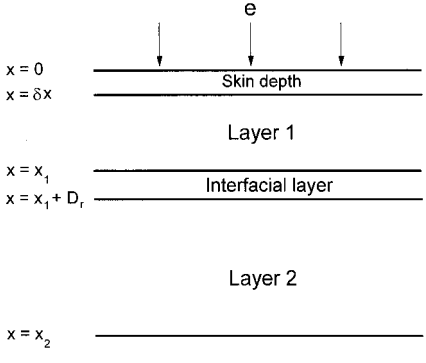

Figure 1. Schematic diagram of the physical system.

For convenience, in the subsequent analysis, the nondimensional variables are defined in the transformed system as follows:

$$x^* = \frac{c_1 x}{2\alpha_1} \qquad t^* = \frac{c_1^2 t}{2\alpha_1} \qquad T_j^* = \frac{T_j - T_0}{T_{\mathrm{ref}}} \qquad q_j^* = \frac{\alpha_1 q_j}{T_{\mathrm{ref}} k_1 c_1} \tag{4}$$

and the dimensionless property ratios

$$\alpha_j^* = \frac{\alpha_j}{\alpha_1} \qquad \tau_j^* = \frac{\tau_j}{\tau_1} \qquad k_j^* = \frac{k_j}{k_1} \tag{5}$$

where $j = 1$, r, and 2 represent layer 1, the interfacial layer, and layer 2, respectively. Clearly, we have $\alpha_1^* = \tau_1^* = k_1^* = 1$. The energy equation and non-Fourier constitutive equation are expressed in terms of the above dimensionless variables as (with asterisks omitted)

$$\frac{\partial T_j}{\partial t} + \frac{1}{k_j}\frac{1}{\alpha_j}\frac{\partial q_j}{\partial x} = 0 \tag{6}$$

$$\frac{\partial q_j}{\partial t} + \frac{k_j}{\tau_j}\frac{\partial T_j}{\partial x} = -2\frac{1}{\tau_j} q_j \tag{7}$$

Equations (6) and (7) can be written in dimensionless vector form as

$$\frac{\partial \mathbf{U}_j}{\partial t} + \frac{\partial \mathbf{F}_j}{\partial x} = \mathbf{S}_j \tag{8}$$

where

$$\mathbf{U}_j = \begin{Bmatrix} T_j \\ q_j \end{Bmatrix} \qquad \mathbf{F}_j = \begin{Bmatrix} \dfrac{1}{k_j}\dfrac{1}{\alpha_j} q_j \\ \dfrac{k_j}{\tau_j} T_j \end{Bmatrix} \qquad \mathbf{S}_j = \begin{Bmatrix} 0 \\ -2\dfrac{1}{\tau_j} q_j \end{Bmatrix} \tag{9}$$

Equation (8) can be written as

$$\frac{\partial \mathbf{U}_j}{\partial t} + [A]_j \frac{\partial \mathbf{U}_j}{\partial x} = \mathbf{S}_j \tag{10}$$

and the Jacobian matrices are

$$[A]_j = \frac{\partial \mathbf{F}_j}{\partial \mathbf{U}_j} \tag{11}$$

Then $[A]_j$ can be diagonalized through the eigenvectors

$$[A]_j = [R]_j [\lambda]_j [R]_j^{-1} \tag{12}$$

where λ denotes the diagonal matrices consisting of two eigenvalues of $[A]$ for each layer. The superscript -1 represents the inverse eigenmatrix. The diagonal matrices and the right eigenmatrices indicate that

$$[\lambda]_j = \begin{bmatrix} -\left(\frac{\alpha_j}{\tau_j}\right)^{1/2} & 0 \\ 0 & \left(\frac{\alpha_j}{\tau_j}\right)^{1/2} \end{bmatrix} \tag{13}$$

$$[R]_j = \begin{bmatrix} 1 & 1 \\ -k_j\left(\frac{1}{\alpha_j}\frac{1}{\tau_j}\right)^{1/2} & k_j\left(\frac{1}{\alpha_j}\frac{1}{\tau_j}\right)^{1/2} \end{bmatrix} \tag{14}$$

The continuities for both temperature and heat flux are imposed as the boundary conditions of the interfacial layer at the interfaces with layer 1 and layer 2, i.e.,

$$T_1 = T_r \qquad q_1 = q_r \qquad x = x_1 \tag{15a}$$

and

$$T_2 = T_r \qquad q_2 = q_r \qquad x = x_1 + D_r \tag{15b}$$

In this study the total nondimensional length is set to unity. In addition, the nondimensional length of layer 2 is set to 0.5. Thus the value of $x_1 + D_r$ in Eq. (15*b*) is 0.5. The dimensionless initial conditions are given as

$$t = 0 \qquad T = q = 0 \tag{16}$$

Moreover, at time $= 0^+$ the dimensionless thermal energy ε_d of width δ_x is released. Release of the thermal disturbance leads immediately to an additional initial condition for the temperature

$$\int_0^{\delta_x} T\,dx = \varepsilon_d \qquad T = \begin{cases} \dfrac{\varepsilon_d}{\delta x} & 0 \le x \le \delta x \\ 0 & \text{otherwise} \end{cases} \qquad t = 0 \tag{17}$$

$$\varepsilon_d = \frac{ec_1}{2\rho_1 C_{p1}\alpha_1 T_{\text{ref}}} \tag{18}$$

The two external boundaries are insulated for all time $t > 0$, i.e.,

$$q_1 = 0 \qquad x = 0 \tag{19a}$$

and

$$q_2 = 0 \qquad x = 1 \tag{19b}$$

NUMERICAL METHOD

This study uses the characteristics-based numerical method developed by Yang [22] to solve the system of equations. First, multiply Eq. (10) by $[R]_j^{-1}$; then obtain

$$\frac{\partial \mathbf{W}_i}{\partial t} + \frac{\partial \mathbf{M}_i}{\partial x} = \mathbf{G}_j \tag{20}$$

where

$$[W]_j = \begin{bmatrix} W^- \\ W^+ \end{bmatrix} = [R]_j^{-1} \cdot [U]_j \qquad [M]_j = [\lambda]_j \cdot [W]_j \qquad [G]_j = [R]_j^{-1} \cdot [S]_j \tag{21}$$

The W_j^- and W_j^+ represent the waves propagating to the negative and positive x directions, respectively. Then, Eq. (20) is expanded by the finite difference and explicit method; therefore we have

$$\mathbf{W}_i^{\text{iter}} = \mathbf{W}_i^n - \frac{\Delta t}{\Delta x}(\mathbf{M}_{i+1/2} - \mathbf{M}_{i-1/2}) + \Delta t \mathbf{G}_i^{\text{iter}} \tag{22}$$

where $\Delta x = x_{i+1/2} - x_{i-1/2}$ and $\Delta t = t^{n+1} - t^n$. Superscript "iter" denotes the iteration value at a new time step of $(n+1)$.

Now the problem attempts to solve the characteristics variable $[W]$ instead of the original T and q coupled equation. Once $[W^{\text{iter}}]$ is known, the iteration values of T and q at time $(n+1)$ can be evaluated by

$$[U^{\text{iter}}] = \begin{Bmatrix} T^{\text{iter}} \\ q^{\text{iter}} \end{Bmatrix} = [R] \cdot [W^{\text{iter}}] \tag{23}$$

It appears that the specified T and q are required to transfer into the characteristic variable W (see Eqs. (9) and (21)). However, there are no specified T and q at the interfaces of $x = x_1$ and $x_1 + D_r$. In addition, only q is specified at the boundaries of $x = 0$ and 1. These two barriers to solving the characteristics variable are treated in the following numerical algorithm:

1. Compute the values of $[G]_j$ and $[W]_j$ at time step $(n+1)$ using Eq. (21).
2. Determine the $[W^+]_1$ and $[W^-]_2$ by using the characteristics equation, Eq. (22). Notably, the TVD scheme [22] is used to compute the characteristics variable $[W]$ at the interior points. In addition, the simple Godunov upwind scheme [23] is employed to compute the $[W]$ value at the point next to the boundaries. The new iteration values of $[W^+]_1$ and $[W^-]_2$ are obtained at time step $(n+1)$ with the exception of the values on the boundaries of $x = 0$ and $x = 1$.
3. Transfer the continuity temperature and heat flux interface conditions of Eq. (15) into characteristic variables W. The two interface equations that

contain the four unknown W variables can be solved when two W values are assigned. Thus the new iteration values of $[W^+]_2$ and $[W^-]_r$ at the interface of $x = x_1 + D_r$, which relates to the new iteration $[W^-]_2$ value and the old iteration $[W^+]_r$ value, are achieved. Likewise, the new iteration values of $[W^-]_1$ and $[W^+]_r$ at the interface of $x = x_1$, which relates to the new iteration $[W^+]_1$ value and the old iteration $[W^-]_r$ value, are also obtained.

4. Take the same procedure as in step 2 to evaluate the new iteration values of $[W^+]_2, [W^-]_r, [W^-]_1$, and $[W^+]_r$ at time step $(n+1)$.
5. Eliminate the unknown temperature variable at the boundaries of $x = 0$ and $x = 1$ by using Eq. (21) to acquire the new iteration values of $[W^+]_1$ at $x = 0$ and $[W^-]_2$ at $x = 1$.
6. Get all the new iteration values of T and q at time step $(n+1)$ in the composite medium by using Eq. (23).

Procedures 1–6 are repeated for time step $(n+1)$ until the T and q values in the composite medium are valid for the criterion of convergence:

$$\left|\frac{T - T^{\text{iter}}}{T}\right|_{\max} \leq 10^{-7} \qquad \left|\frac{q - q^{\text{iter}}}{q}\right|_{\max} \leq 10^{-7} \tag{24}$$

Then the values of T and q at time $(n+1)$ can be fully evaluated.

RESULTS AND DISCUSSION

The study focuses on thermal wave propagation in a composite medium with boundary resistance at the interface. To consider the interface resistance, the interfacial layer model is employed [19–21]. This model assumes a layer of a variable thickness ($D_r \sim 1$–10% of the layer 1 thickness x_1), where the conductivity is significantly lower than that of layer 1 ($k_r \sim 1$–10% of the layer 1 conductivity k_1). The remaining properties (α and τ) are the same as in layer 1. In addition, the pulsed incident energy is absorbed by skin depth $\delta x = 0.05$ adjacent to the exterior surface at $x = 0$. By choosing T_{ref} as $ec_1/\rho_1 C_{p1}\alpha_1$, we obtain

$$T = \begin{cases} 10 & 0 \leq x \leq 0.05 \\ 0 & \text{otherwise} \end{cases} \qquad t = 0^+ \tag{25}$$

A one-dimensional computer code was written on the basis of the above calculation procedure. Grid refinement and time step sensitivity studies have also been performed for the physical model to ensure that the essential physics are independent of grid size and time interval. The physical domain reduces to become a finite medium when layer 1 and layer 2 embody the same material properties and the interface is in perfect contact. The analytical solution of the finite medium has been given by Özisik and Vick [24] and is used to demonstrate the validity of the numerical solutions in this study. Figure 2 is a comparison of the numerical and analytical solutions in a finite medium. The numerical solutions clearly exhibit free

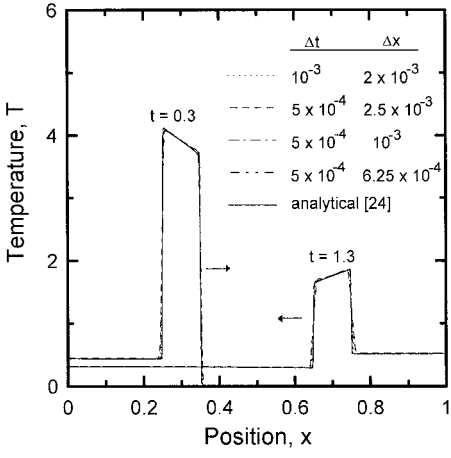

Figure 2. Comparison of numerical and analytical temperature in a finite medium at $t = 0.3$ and 1.3.

oscillations around the sharp discontinuity. In addition, the dissipation error at the wave front is almost invisible when a grid size less than 10^{-3} with a time interval of 5×10^{-4} is utilized. Therefore the uniform 1000 grid system with $\Delta t = 5 \times 10^{-4}$ is used to generate the presented results. Corresponding to the step sizes in space and time, the Courant number $\Delta t/\Delta x$ is 0.5.

Figure 3 illustrates the temperature distribution for both perfect contact interface and imperfect contact cases at $t = 0.1$ and 0.7. The hyperbolic heat

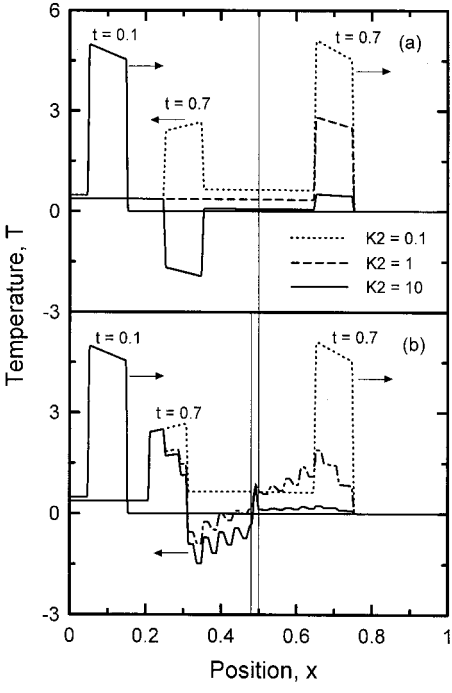

Figure 3. Temperature distributions at $t = 0.1$ and 0.7, $\alpha_2 = \tau_2 = 1$ for (a) the perfect contact case and (b) the thermal resistance existence case, $D_r = 0.02$, $k_r = 0.1$.

conduction equation predicts that a thermal wave disturbance tends to propagate in a given direction until its course is impeded by a wall or barrier. When the temperature is suddenly increased to 10 within δx at $t = 0^+$, a thermal wave is generated and propagates. Initially, owing to the reflection of the pulse wave from the insulated surface at $x = 0$, the wave width is doubled. This gives the leading edge of the wave-front impact at the contact interface at $t = 0.45$ and $(0.45 - D_r)$ for a perfect contact and an imperfect contact interface, respectively. At $t = 0.7$ a reflected wave traveling toward the left and a transmitted wave traveling toward the right are observed. For a perfect contact case, both waves retain the initial waveform and k_2 affects their strength, as evidenced in Figure 3*a*. The reflected waves in layer 1 may be positive or negative in magnitude, depending on the thermal conductivity ratio of two layers, which is consistent with energy conservation. The results are analogous to those in the analysis of Frankel et al. [15] for an initial pulsed volumetric source. Figure 3*b* presents the results for an imperfect contact interface. The wave feature at $t = 0.1$ is identical to the perfect contact case, as attributed to the fact that the wave front is unaware of the thermal barrier. However, it shows the interface resistance significantly influences the wave pattern and strength after the initial wave impact of the interface. The secondary wavelets behind the reflected and transmitted wave are observed for $k_2 = 1$ and 10 but do not exist for $k_2 = 0.1$ because the interfacial layer with $k_r = 0.1$ becomes a part of layer 2. This explains that the wavelets are induced by the interfacial layer instead of the numerical instabilities. The remaining figures thoroughly describe reflection and transmission phenomena with interface resistance.

Figures 4 and 5 display the heat flux and temperature distribution, respectively, at various time intervals when the interfacial layer exists at the interface. At $t = 0.1$ the leading edge of the wave locates at $x = 0.15$. With an increase of time, the traveling wave approaches the interface of the composite. Most of the energy is reflected back when the initial wave impacts the interfacial layer due to $k_r \ll k_1$. The wave transmitted through x_1 further divides into two waves when it impacts the surface at $x_1 + D_r$. One wave reflects back toward surface x_1, while the other transmits into layer 2. For each time interval of 0.02, a situation when the wave in the interfacial layer impacts the interface with layer 1 or 2 causes a transmitted wave to travel into layer 1 or layer 2. This subsequently leads to secondary wavelets in both layers (Figures 4*b* and 4*c*). The secondary wavelets are continuously transmitted from the interfacial layer with the strength decreasing with time due to the energy exchanged with both layers. Since the heat capacity of ρC_p changes in proportion to k when α is held constant, the nature of the wave for the temperature distribution in layer 2 is insignificant (Figures 5*b* and 5*c*). After the wave is reflected by the external insulated boundaries, the heat flux wave is converted into an inverse wave front (Figure 4*d*). In addition, the temperature wave retains the original wave sign (Figure 5*d*), moving toward the center of the composite. At this moment, diffusion dominates the heat transfer in the interfacial layer. According to Figures 4*e* and 5*e*, the reflection and transmission at the interfaces of the interfacial layer occur again by $t = 1.7$. The reflection-transmission combination persists until diffusion dominates in both layers.

In light of the experiments in superfluid helium [25], the initial waveform is modified by the reflected waves at the interface of dissimilar materials. The

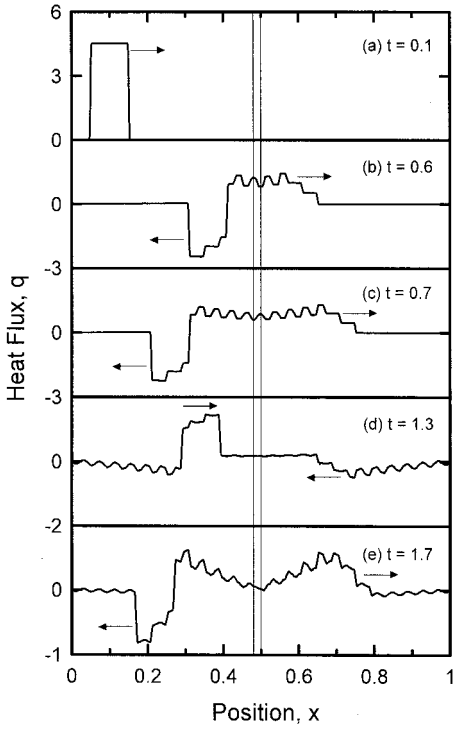

Figure 4. Heat flux distributions for a sequence of times with $D_r = 0.02$, $k_r = 0.05$, $\alpha_2 = \tau_2 = 1$, and $k_2 = 10$.

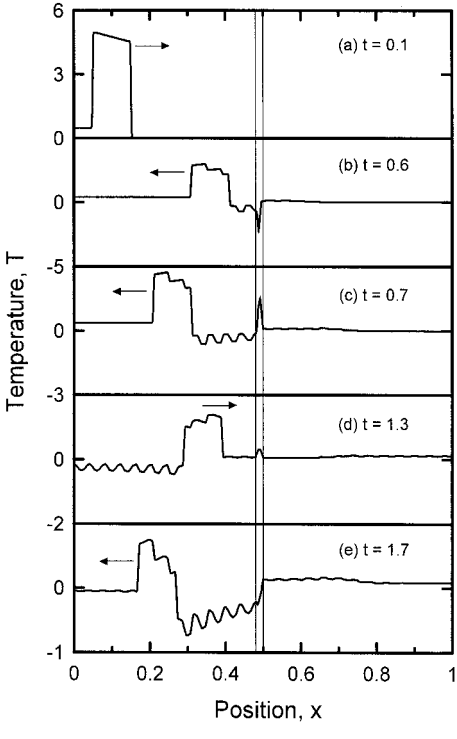

Figure 5. Temperature distributions for a sequence of times with $D_r = 0.02$, $k_r = 0.05$, $\alpha_2 = \tau_2 = 1$, and $k_2 = 10$.

superfluid helium is characterized as a mixture of two fluid components: the normal and super components. The vortex layer between the normal and super components is produced when a strong second sound shock wave passes through the fluid [25, 26]. It can be hypothesized that the interfacial layer that mediates the exchanges of energy between two dissimilar layers is the vortex layer that mediates the exchanges of momentum layer between the two fluid components. The waveform of the secondary wavelets traveling behind the reflected and transmitted wave resembles that of the experimental observation in superfluid helium [25].

Figure 6 depicts a sequence of temperature distributions with only a slight time interval change to understand the wave nature within the interfacial layer and the interaction with the incoming wave from the neighborhood. Because of the dissipation of energy by diffusion, a slant across the top of the wave ($\partial T/\partial x < 0$) is presented in Figure 6*a*. At $t = 0.43$, the leading edge of the original wave impacts the surface at x_1. Owing to the wave width being 0.1, it takes 0.1 dimensionless time for the initial wave to complete the interaction at x_1. The superposition of the reflected wave by the interfacial layer with the original wave increases the temperature at $x = x_1$ (Figure 6*b*). Meanwhile, a positive temperature wave transmits into the interfacial layer (Figure 6*c*). Once the transmission wave impacts the surface at $x_1 + D_r$, the reflection-transmission phenomena occur again. The temperature wave in the interfacial layer disappears owing to the combination of the transmitted positive-sign wave from x_1 with the negative-sign

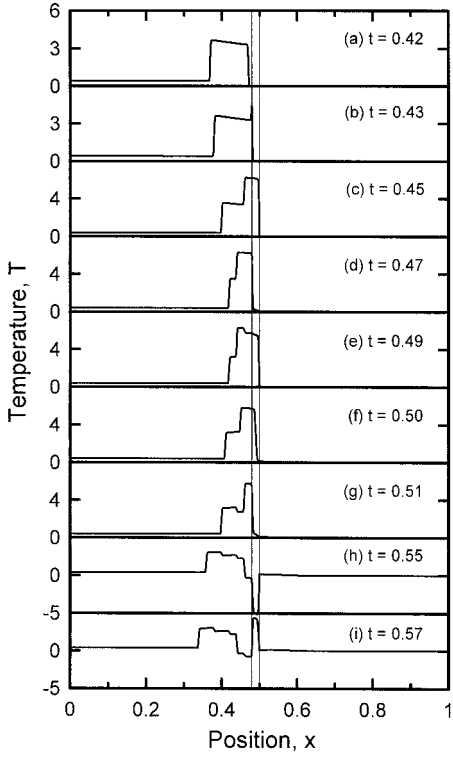

Figure 6. Temperature distributions for a sequence of times with $D_r = 0.02$, $k_r = 0.05$, $\alpha_2 = \tau_2 = 1$, and $k_2 = 10$ demonstrating the interaction of thermal waves in the interfacial layer and an initial pulsed wave.

reflected wave from $x_1 + D_r$ (Figure 6*d*). The positive temperature wave periodic appears and disappears in the interfacial layer for a time interval of D_r (Figures 6*e*–6*g*). Moreover, the transmitted negative wave through x_1 into layer 1 weakens the incoming wave, resulting in deformation of the reflected wave feature. By $t = 0.55$, the initial wave from layer 1 has completed the interaction with the interfacial layer at x_1, and no positive-sign wave was transmitted into the interfacial layer to depress the negative-sign wave reflected from $x_1 + D_r$. The temperature wave in the interfacial layer changes sign for the 0.02 time interval (Figures 6*h* and 6*i*) and transmits into layer 1 to produce the secondary wavelets in the wake of the reflected wave until diffusion dominates in the interfacial layer.

Figure 7 together with Figure 3*b* display the effects of k_2 and k_r on the temperature distribution at $t = 0.7$. Owing to the fact that the energy is an integral of $\rho C_p T$, the induced temperature distribution in layer 1 and 2 (which correspond to the energy transmitted from the interfacial layer) depend on their conductivity when diffusivity is held constant. Therefore the secondary temperature wavelets are significant in layer 2 when $k_2 < 1$ and are significant in layer 1 when $k_2 > 1$. The secondary temperature wavelets are observed in both layers when $k_2 = 1$. In addition, when k_2 approximately equals k_r, the interfacial layer becomes part of layer 2. This leads the secondary wavelets to disappear; meanwhile, the reflected and transmitted waves retain the initial wave feature. Moreover, the magnitude of the temperature in the interfacial layer increases with a decrease of k_r.

Figure 8 illustrates the effect of k_r on the average temperature of layer 2. The leading edge of the initial pulsed wave front impacts at the interface of

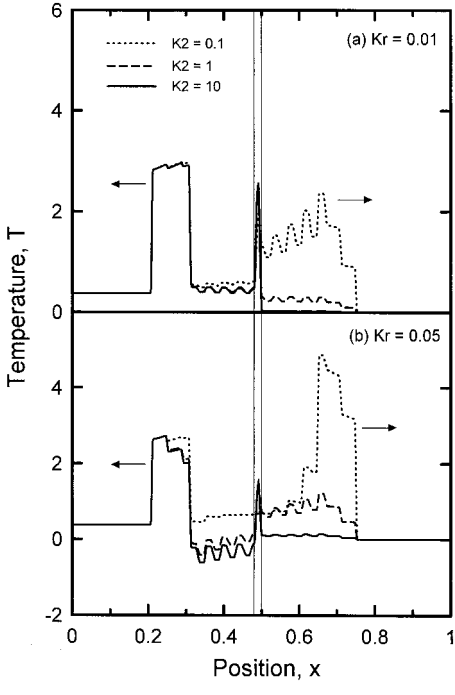

Figure 7. Effect of k_r on temperature at $t = 0.7$ with $D_r = 0.02$ and $\alpha_2 = \tau_2 = 1$.

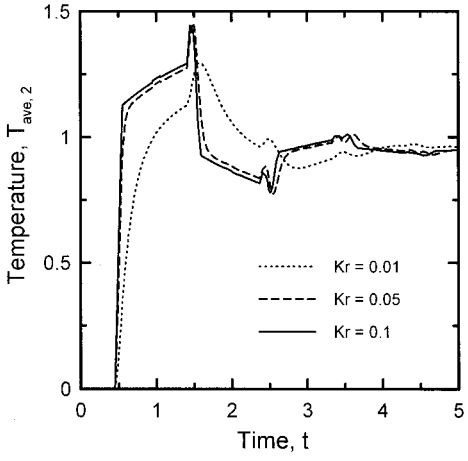

Figure 8. Effect of k_r on $T_{\text{ave},2}$ with $D_r = 0.02$, $\alpha_2 = \tau_2 = 1$, and $k_2 = 0.1$.

$x = 0.5$ at $t = 0.45$. After a dimensionless time interval of 1, the waves reflected by the exterior insulated surfaces impact the surface again. At these moments the $T_{\text{ave},2}$ abruptly changes. For the remaining times the average temperature gradually changing with time is attributed to the fact that the residual energy in the wake of the propagating wave exchanges a slight amount of energy across that surface. The energy passing through the interfacial layer to enter layer 2 is directly proportional to k_r, thereby causing the higher average temperature in layer 2 for a higher value of k_r at $t = 0.45$. Likewise, more energy passes through this surface to enter layer 1 for a higher value of k_r when the waves are reflected by the exterior surfaces and impact the surface at $x = 0.5$. Thus $T_{\text{ave},2}$ increases and decreases with changes in k_r for a time interval of 1. The effect of k_r on $T_{\text{ave},2}$ becomes less serious with an increase of time, since the diffusion dominates in the composite medium.

Figures 9 and 10 illustrate the effect of diffusivity and relaxation time of layer 2 on the reflected wave and transmitted wave at $t = 0.7$. In the transmitted portion, Figure 9 displays the effects of α_2 on the transmitted wave in two ways.

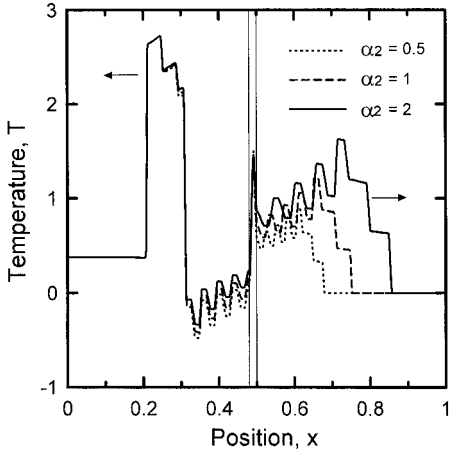

Figure 9. Effect of α_2 on temperature at $t = 0.7$, with $D_r = 0.02$, $k_r = 0.05$, and $k_2 = \tau_2 = 1$.

The width of the wave at a standard case of $\alpha_2 = 1$ has been expanded for $\alpha_2 > 1$ due to the speed $c_2 = (\alpha_2/\tau_2)^{1/2}$ becoming faster than 1. Meanwhile, the strength of the wave is amplified for $\alpha_2 > 1$ for energy conservation. The opposite situation occurs when $\alpha_2 < 1$. The effect of τ_2 on the transmitted wave presented in Figure 10 is also based on the energy conservation and wave speed changes with relaxation time τ. These phenomena resemble those demonstrated in the perfect contact problems [15]. In the reflected portion of Figures 9 and 10, owing to the fact that the wave speed in the interfacial layer is independent of the variation of α_2 and τ_2, the interfacial-layer-induced secondary wavelet behind the reflected wave travels with the same speed toward the origin. The magnitude of the secondary wavelets increases with the decrease of α_2 and τ_2.

Figure 11 illustrates the influences of interfacial layer thickness D_r on the temperature distributions with two different values of k_2 at $t = 0.7$. The initial pulse wave takes 0.1 dimensionless time to complete the reflection and transmission at x_1. Within this time interval, the reflection-transmission-combinatio n phenomena in the interfacial layer assess the reflected and transmitted wave figures and their strength. The transmitted wave through x_1 traveling right couples with more of the positive wave, which is the reflected wave of the negative wave traveling left from $x_1 + D_r$ when D_r is less thick. Consequently, the transmitted wave strength in layer 2 increases with decreasing D_r; the opposite occurs for a reflected wave in layer 1. The initial pulse wave completes the reflection and transmission at x_1 before the reflected wave from $x_1 + D_r$ arriving in this surface when D_r is equal, or greater than the absorption skin depth δx (i.e., $D_r \geq 0.05$). Therefore the reflected wave retains the initial wave feature. Moreover, when the interfacial thickness is very thin, the piecewise secondary wavelets become smooth.

Figure 12 illustrates the discrepancies of the maximum temperature in layer 2 at $t = 0.7$ between the perfect contact and imperfect contact interface. The maximum temperature in layer 2 is located at the trailing edge of the transmitted wave (see Figures 7 and 11). The interfacial layer becomes part of layer 2 when $k_r = k_2$. Thus the solutions are independent of the interfacial layer thickness. A decrease of k_r dramatizes the effect of resistance to cause less energy to enter

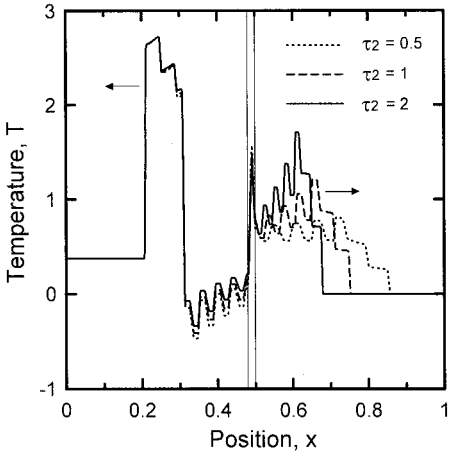

Figure 10. Effect of τ_2 on temperature at $t = 0.7$ with $D_r = 0.02$, $k_r = 0.05$, and $k_2 = \alpha_2 = 1$.

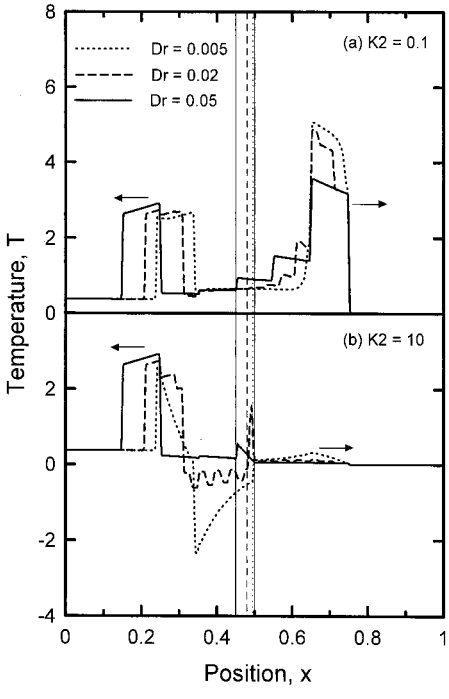

Figure 11. Effect of D_r on temperature at $t = 0.7$ with $k_r = 0.05$, and $\alpha_2 = \tau_2 = 1$.

layer 2. However, loss in the transmitted wave strength caused by k_r is compensated by the waves' transmission-reflection-combination phenomena in the interfacial layer for a very thin interfacial thickness, such as $D_r = 0.005$. This causes the $T_{\max}$ in layer 2 to become nearly independent of the variation of k_r for $D_r = 0.005$. More serious discrepancies arise between different interface conditions where the interfacial layer has a lower conductivity and a higher thickness.

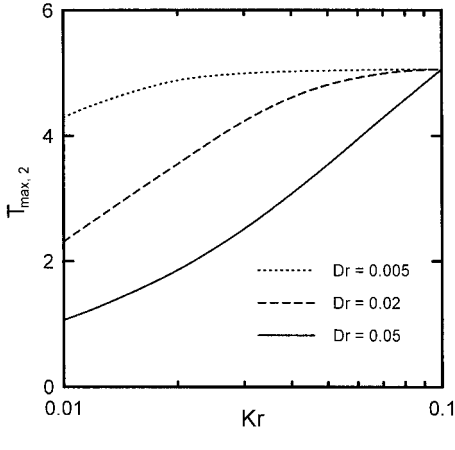

Figure 12. Effect of interface resistance on $T_{\max,2}$ at $t = 0.7$ with $k_2 = 0.1$ and $\alpha_2 = \tau_2 = 1$.

CONCLUSIONS

By applying the hyperbolic heat conduction equation, this study numerically analyzes transient thermal wave propagation in a two-layer composite medium with an initial temperature pulse emanating from one layer. The interfacial layer model is used to examine the thermal boundary resistance. The reflection and transmission at the interface of two dissimilar materials are presented as well.

According to the analysis results, the thermal boundary resistance restricts the exchanges of energy between two dissimilar layers. The relative strengths of the reflected wave and transmitted wave are varied with the conductivity and thickness of the interfacial layer. Less energy transmits from the first layer through the interfacial layer into the second layer for a lower conductivity and a higher thickness of the interfacial layer.

Analysis results further demonstrate that thermal boundary resistance not only mediates the energy transform from one layer to the other, but also markedly influences the thermal wave transmission-reflection-combination phenomena. The wave nature in the interfacial layer deforms the initial wavelike feature and produces secondary wavelets behind the reflected and transmitted waves until the diffusion phenomena dominate. The strength of the secondary wavelets depends on the property ratios of each layer. Moreover, the reflected wave retains the initial wave feature when the interfacial thickness is equal to or greater than the absorption skin depth. Furthermore, the piecewise secondary wavelets smooth when the interfacial layer thickness is very thin.

REFERENCES

1. E. T. Swartz and R. O. Pohl, Thermal Boundary Resistance, *Rev. Mod. Phys.*, vol. 61, pp. 605–668, 1989.
2. R. C. Chen, J. P. Wu, and H. S. Chu, Bolometric Response of High-Tc Superconducting Detectors to Optical Pulses and Continuous Waves, *ASME J. Heat Transfer*, vol. 117, pp. 336–372, 1995.
3. R. J. Von Gutfeld, Heat Pulse Transmission, in W. P. Masoned (ed.), *Physical Acoustics: Principles and Methods*, vol. V, p. 233, Academic, New York, 1973.
4. M. J. Maurer and H. A. Thompson, Non-Fourier Effects at High Heat Flux, *ASME J. Heat Transfer*, vol. 95, pp. 284–286, 1973.
5. D. D. Joseph and L. Preziosi, Heat Wave, *Rev. Mod. Phys.*, vol. 61, pp. 41–73, 1989.
6. D. Y. Tzou, On the Thermal Shock Wave Induced by a Moving Heat Source, *ASME. J. Heat Transfer*, vol. 111, pp. 232–238, 1989.
7. C. Cattaneo, *Sullaconduzione De Calore*, vol. 3, pp. 83–101, Atti del Seminar, Mat. Fis. Univ., Modena, 1958.
8. P. Vernotte, Les Paradoxes de la Theorie Continue de l'Equation de la Chaleur, *Compute Rendus*, vol. 246, pp. 3145–3155, 1958.
9. M. Chester, Second Sound in Solid, *Phys. Rev.*, vol. 131, pp. 2013–2015, 1963.
10. R. E. Nettleton, Relaxation Theory of Thermal Conduction in Liquids, *Phys Fluids*, vol. 3, pp. 216–225, 1960.
11. M. J. Maurer, Relaxation Model for Heat Conduction in Metals, *J. Appl. Phys.*, vol. 40, pp. 5123–5130, 1969.
12. H. P. Francis, Thermo-Mechanical Effects in Elastic Wave Propagation: A Survey, *J. Sound Vibration*, vol. 21, pp. 181–192, 1972.

13. K. Mitra, S. Kumar, A Vedavarz, and M. K. Moallemi, Experimental Evidence of Hyperbolic Heat Conduction in Processed Meat, *ASME J. Heat Transfer*, vol. 117, pp. 568–573, 1995.
14. M. N. Özisik, and D. Y. Tzou, On the Wave Theory in Heat Conduction, *ASME J. Heat Transfer*, vol. 116, pp. 526–535, 1994.
15. J. I. Frankel, B. Vick, and M. N. Özisik, General Formulation and Analysis of Hyperbolic Heat Conduction in Composite Media, *Int. J. Heat Mass Transfer*, vol. 30, pp. 1293–1305, 1987.
16. D. Y. Tzou, Reflection and Refraction of Thermal Waves from a Surface or an Interface Between Dissimilar Materials, *Int. J. Heat Mass Transfer*, vol. 36, pp. 401–410, 1993.
17. C. Bai and A. S. Lavine, Thermal Boundary Conditions for Hyperbolic Heat Conduction: Heat Transfer on the Microscale, *ASME 1993*, HTD-vol. 253, pp. 37–44, 1993.
18. S. K. Streiffer, B. M. Lairson, C. B. Eom, B. M. Clemens, J. C. Bravman, and T. H. Geballe, Microstructure of Ultrathin Films of $YBa_2Cu_3O_{7-\delta}$ on MgO, *Phys. Rev. B*, vol. 43, pp. 13007–13018, 1991.
19. C. D. Marshall, I. M. Fishman, R. C. Dorfman, C. B. Eom, and M. D. Fayer, Thermal Diffusion, Interfacial Thermal Barrier, and Ultrasonic Propagation in $YBa_2Cu_3O_7$ Thin Films: Surface-Selective Transient-Grating Experiments, *Phys. Rev. B*, vol. 45, pp. 10009–10021, 1992.
20. A. K. Das and S. S. Sadhal, Effect of Interstitial Fluid on Thermal Constriction Resistance, *ASME J. Heat Transfer*, vol. 114, pp. 1045–1048, 1992.
21. A. K. Das and S. S. Sadhal, A Note on the Evaluation of Thermal Constriction Resistance for Finite Thickness Gaps, *ASME J. Heat Transfer*, vol. 119, pp. 177–180, 1997.
22. H. Q. Yang, Characteristics-Based, High-Order Accurate and Nonoscillatory Numerical Method for Hyperbolic Heat Conduction, *Numer. Heat Transfer B*, vol. 18, pp. 221–241, 1990.
23. W. K. Yeung and T. T. Lam, A Numerical Scheme or Non-Fourier Heat Conduction, Part I: One-Dimensional Problem Formulation and Applications, *Numer. Heat Transfer Part B*, vol. 33, pp. 215–233, 1998.
24. M. N. Özisik and B. Vick, Propagation and Reflection of Thermal Waves in a Finite Medium, *Int. J. Heat Mass Transfer*, vol. 27, pp. 1845–1854, 1984.
25. J. R. Torczynski, On the Interaction of Second Sound Shock Waves and Vorticity in Superfluid Helium, *Phys. Fluids*, vol. 27, pp. 2636–2644, 1984.
26. T. Shimazaki, M. Murakami, and T. Lida, Second Sound Wave Heat Transfer, Thermal Boundary Layer Formation and Boiling: Highly Transient Heat Transport Phenomena in He II, *Cryogenics*, vol. 35, pp. 645–651, 1995.